The Iranian Journal of Mechanical Engineering Transactions of ISME
Journal homepage: https://jmee.isme.ir/
Vol. 26, No. 1, 2025, pp. 66-83

Research Paper

DOI: https://doi.org/10.30506/jmee.2024.2014713.1327

Comparative Evaluation of Combustion Mechanisms (GRI 3.0 and DRM19) in MILD Combustor

Mohamad-Amin Zamani[*]
PhD Student

Mohamad-Hassan Saidi[†]
Professor

One of the newest combustion technologies is the MILD combustion process, which is based on preheating fuel and air and diluting the oxygen content of the air to produce a proper mixing of the reactants. In the present study, MILD combustion of methane is simulated in a lab-scale combustor and its results will be compared in two modes of combustion mechanisms, namely DRM19 (as reduced mechanism) and GRI 3.0 (as complete mechanism). The results show that both mechanisms have uniform temperature distribution, diluting of oxygen reaches to below 5% and the amount of NOX and CO pollutants is reduced to below 10ppm. However, based on the solution procedure, the DRM19 mechanism has higher accuracy and convergence speed compared to GRI 3.0.

Keywords: MILD combustion, Fossil fuel, Gaseous pollutants, Combustion mechanism

1 Introduction

Combustion is defined as a chemical reaction in which a certain amount of fuel and air, as reactants, are combined and the combustion products are generated as various chemical species with the release of a large amount of energy in the form of light and heat. Emission of large amounts of gaseous pollutants such as nitrogen oxides (NO_X), carbon monoxide (CO), unburned hydrocarbons (HC) and climate changes, such as excessive warming of the earth with the emission of carbon dioxide (CO_2) as a greenhouse gas, are the negative effects of fossil fuel combustion. To enhance the efficiency and quality of the combustion processes, it is necessary to develop new methods[1]. These technologies include swirl burners, oxy-fuel fuel-oxygen burners, staged combustion, and cooling flame.
MILD[‡] combustion technology is a new combustion method. In Wünning's experiments, this phenomenon was first observed [2, 3].

[*]PhD Student, Faculty of Mechanical Engineering, Sharif University of Technology, Tehran, Iran, zamani.m_amin@mech.sharif.edu
[†]Corresponding author, Professor, Faculty of Mechanical Engineering, Sharif University of Technology, Tehran, Iran, saman@sharif.edu
[‡]Moderate or Intense Low Oxygen Dilution

Received: 2023/10/30, Revised: 2024/09/20, Accepted: 2024/11/24

During his experiments on a regenerative burner with a temperature of 1000 ℃ and preheated air at 650 ℃, it was observed that the fuel was completely consumed without showing a visible flame. It was discovered that the stack had a negligible amount of carbon monoxide and nitrogen oxides during stable and mild combustion.

To achieve MILD combustion, the fuel and air must be preheated to a temperature higher than the auto-ignition temperature of the fuel; in such a way that the combustion temperature (difference between reactants and products) is lower than the auto-ignition temperature of the fuel, and the oxygen in the air must be diluted to below 10% of its initial value, Due to the proper mixing of fuel and air in this regime, it is possible to create a homogeneous combustion zone with uniform temperature, in which the fuel consumption, the rate of production of gas pollutants, specifically NOx and CO, are reduced and the efficiency of the system is increased. The recirculation of hot gases of combustion is a key issue in the MILD combustion process, by which the reactants can be preheated, through direct or indirect heat exchange, and the airflow be diluted i.e. the mole fraction of oxygen be decreased in the air through the combination of reactants with combustion products, and by increasing the residence time of the products, causes proper mixing of fuel and air; thus no unburned fuel or no excess oxygen remains in the combustion chamber.

The dimensionless number Kv is used to define the amount of recirculation of hot gases as follows [4, 5]:

$$K_v = \frac{M_E}{M_F + M_A} \tag{1}$$

where "M" is the mass flow rate, "E" is the exhaust gases of the regenerator, "F" is the fuel, and "A" is the air.

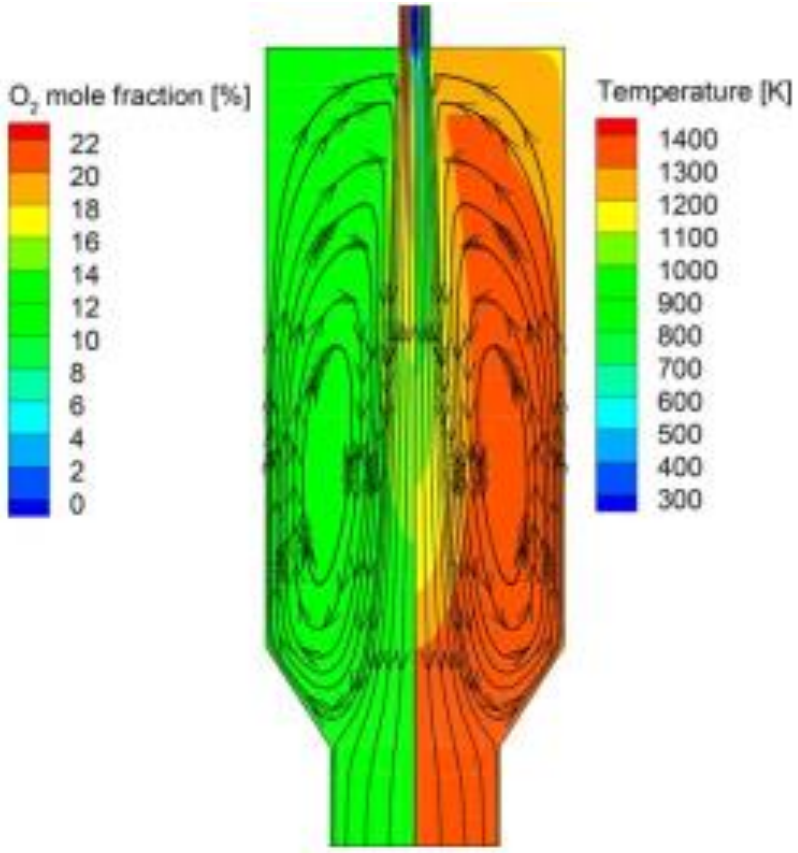

Figure 1 The contour of the mole fraction of oxygen, temperature, and flow pattern [2]

Jeon and Kim[6] investigated the effect of the mixing coefficient of the MEPDF model equation on the formation of MILD combustion and compared the obtained data with experimental data. They used GRI 2.11 mechanism (49 species and 279 elementary reactions). They found that the recirculation rate decreases with increasing the mixing coefficient of the MEPDF equation, which was 2.01, 1.94, and 1.82 for the coefficients of 0.5, 0.15, and 0.2, respectively. Their conclusion was that increased recirculation results in an increase in combustion area, while a decrease in oxygen concentration is observed. From the contour of temperature, they concluded that the reduction of the mixing coefficient increases the recirculation rate of combustion products, and as a result, the maximum temperature and temperature gradient decrease. They also found that the central region expands with low temperatures due to the reduction of the mixing coefficient; because the auto-ignition time and the combustion process are delayed due to the weakening of the mixing of combustion products and inputs. The reduction of the mixing coefficient of the MEPDF equation causes the mixing between the species to become less and weaker, the recirculation increases, and as a result, the excess temperature decreases and the temperature zone expands.

Cheong et al.[7] investigated the effect of changing the arrangement of propane and air nozzles and the distance between nozzles on creating MILD combustion in a laboratory furnace. Their results showed that in lower equivalence ratios where oxygen is more concentrated, the distribution of temperature and heat flux is more non-uniform, and it is more difficult to create MILD combustion. In order to mix well, the intake air and fuel must be close to each other. When the mixture is nearer to stoichiometric composition and the oxygen concentration is lower, the temperature distribution and heat flux become more uniform. MILD combustion can occur at long distances from nozzles as well. The contours of the internal recirculation zone show that at a far distance between two nozzles, the fuel and air must be first mixed with the combustion products of the reaction and then developed in the recirculation zone. Due to the smaller recirculation area, creating MILD combustion at far distances from nozzles has become more challenging.

Zhiyi Li et al.[8] compared the ability of two combustion models, namely EDC* and PaSR† in creating MILD combustion in a 10 kW laboratory scale furnace and compared the results with the experimental tests. According to their findings, PaSR's prediction of average temperature and carbon dioxide values is less accurate than the experimental test, while EDC predicts more accurate values than the experimental test. The mixing coefficient calculation procedure is the main cause of the difference between these two combustion models.

Previous numerical studies have less frequently investigated the effect of chemical reaction mechanism selection on simulation accuracy. Since the chemical reaction mechanism outlines the reaction pathway, it can influence the results. Although this effect might be less significant than the choice of numerical models, it substantially affects computational run time. Various chemical mechanisms have been developed, but this paper focuses on investigation of performance of a complete mechanism (GRI 3.0) and a reduced mechanism (DRM19). The purpose of the current research is to compare the accuracy of temperature distribution, pollutants, and chemical species predictions made by two distinct mechanisms: GRI 3.0, which is a complete mechanism, and DRM19, which is a reduced mechanism, using numerical simulation of MILD combustion in a laboratory combustion chamber. The run time is increased by complete mechanisms because they have more species and reactions. On the other hand, because there are fewer species and chemical reactions in reduced mechanisms which occur due to the removal of less significant species from complete mechanisms the pace of solution is higher. Reduced mechanisms are unable to forecast certain chemical species, such NO_X. To calculate these species, chemical equilibrium can be used.

*Eddy dissipation concept
†Partially stirred reactor

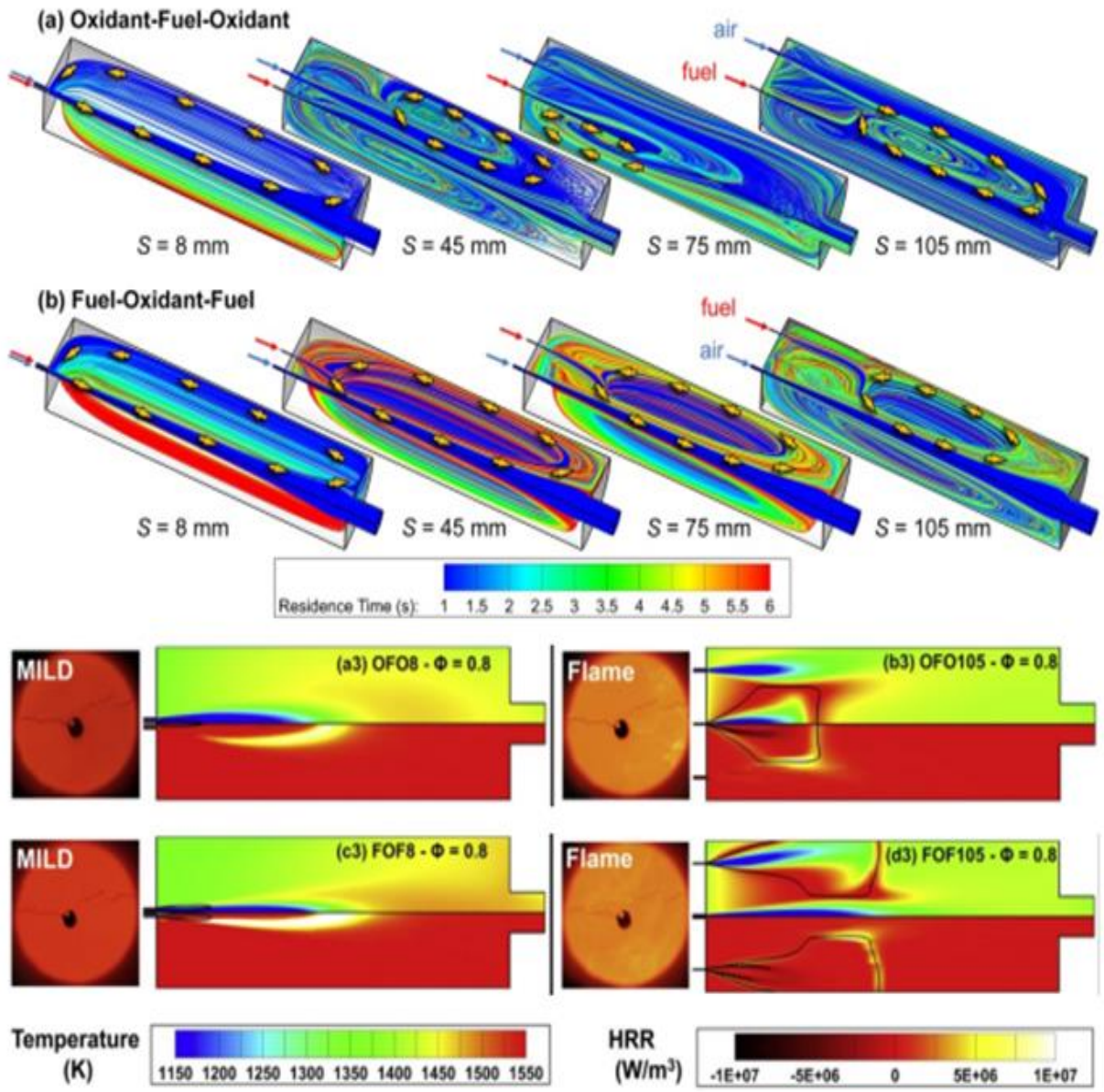

Figure 2 The contour of the internal recirculation area in various situations [3]

2 Geometry and simulation

The present study is carried out based on the Dally furnace[9] shown in Figure (3). This combustion chamber is a rectangular cube with dimensions of 250mm * 250mm * 550mm. It also has a non-premixed fuel and air inlet with a temperature of 306 K and two stacks on the same side of the inlet.

The input values of the above geometry for validation and simulation are given in Table (1).

Figure (4) shows the generated mesh (595,000 cells) taking into account the grid independence criterion. Finer meshes at the wall edges to achieve the appropriate $y+$ range, as well as near inlets and outlets to avoid velocity and pressure gradients. To make it thinner near the inlet and outlet nozzle walls, boundary mesh layers were used.

In this geometry, the wall temperature is 1500 K and no-slip boundary condition is used for the velocity. Furthermore, near the walls, the pressure, temperature, and mass fraction of the species have zero gradient conditions above the boundary conditions of the walls. Additionally, the velocity, kinetic energy, and energy dissipation rate are calculated using wall functions (Figure (5) and Table (2)).

Table 1 Fuel and air intake parameters for simulation [9]

Parameters	Fuel	Air
Chemical compounds+	CH_4	$\%79N_2+\%21O_2$
Temperature(K)	306	306
Mass flow rate (kg/h)	0.68	13.62
Velocity (m/s)	9.32	22.38
Excess air	λ =1.25	

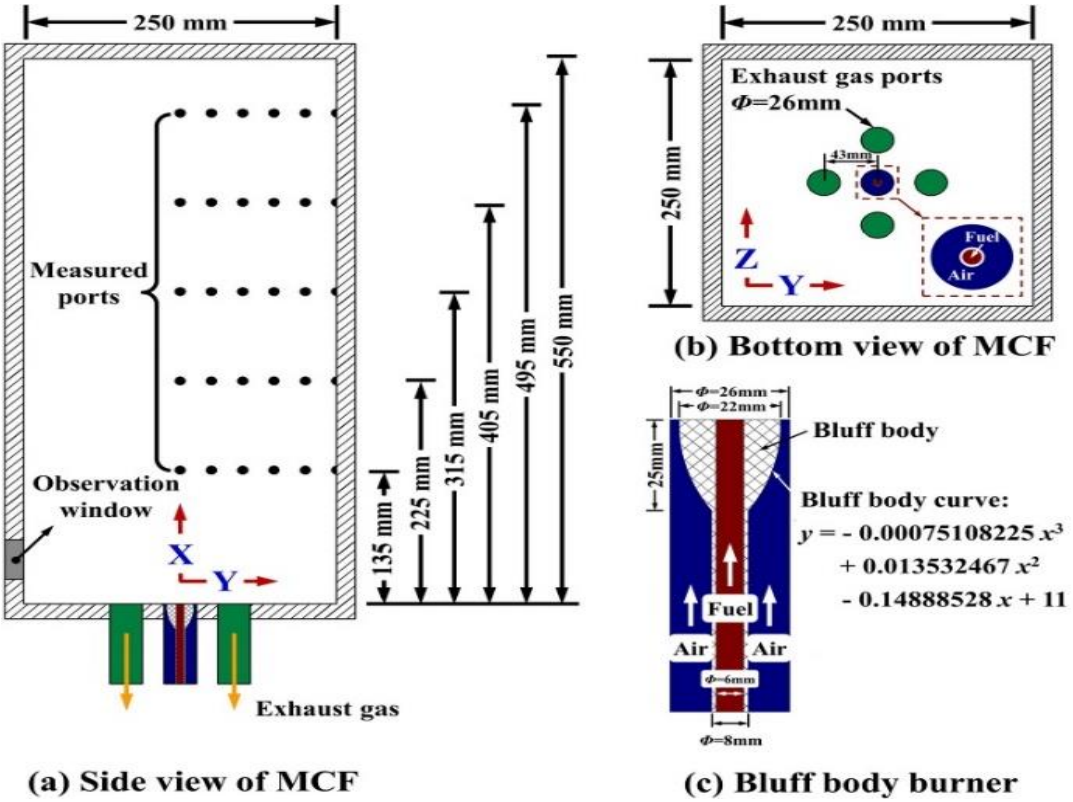

Figure 3 Combustion chamber geometry [9]

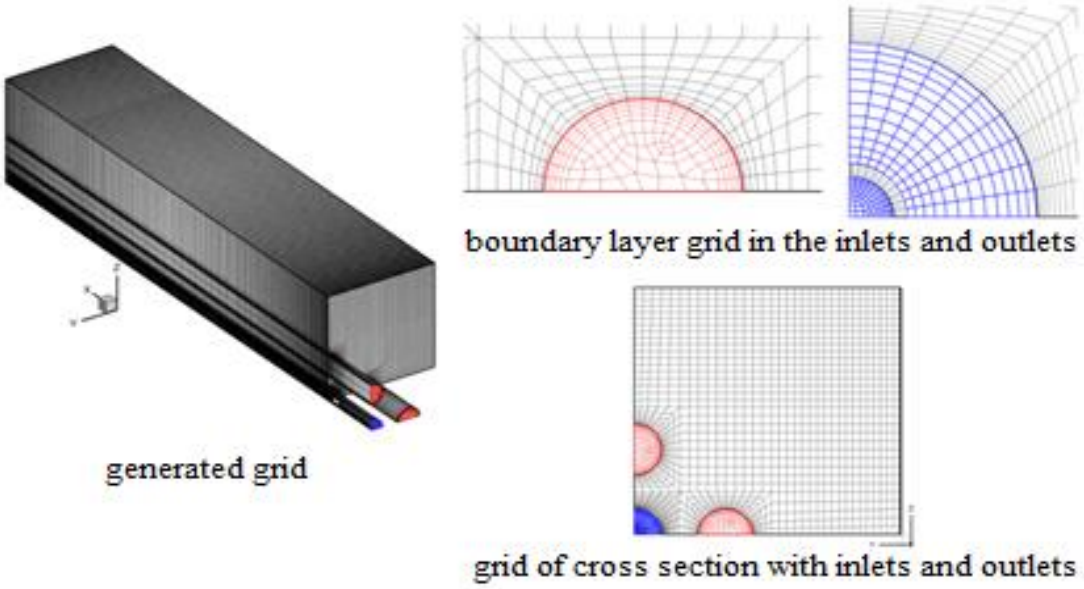

Figure 4 Meshes created in the geometry and their different parts

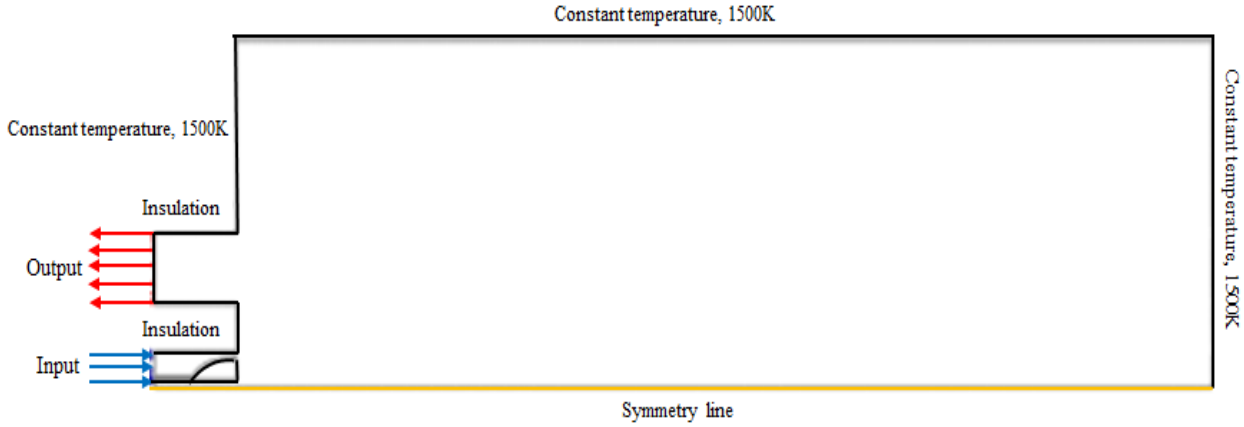

Figure 5 Thermal boundary condition of furnace walls

Table 2 Boundary conditions of simulation

	Input	Output	Walls
Velocity (V)	Known (Table 1)	Calculated by continuity equation	No slip boundary condition and wall functions
Temperature (T)	Known (Table 1)	Must be calculated	Known (Fig. 5)
Pressure (P)	Calculated by Bernoulli's equation	Known (Atmospheric)	Zero gradient ($\nabla P = 0$)
Species (Y_i)	Known (Table 1)	Zero gradient ($\nabla Y_i = 0$)	Zero gradient ($\nabla Y_i = 0$)

3 Governing equations

To study the combustion process, it is necessary to solve four equations: continuity, momentum, energy, and conservation of species as well as chemical reactions given below[10, 11]:

$$\frac{\partial \bar{\rho}}{\partial t} + \nabla \cdot \left(\bar{\rho}\vec{u}\right) = 0 \tag{2}$$

$$\frac{\partial(\bar{\rho}\vec{u})}{\partial t} + \vec{u} \cdot \nabla\left(\bar{\rho}\vec{u}\right) = -\nabla P + \nabla \cdot \left[(\bar{\mu} + \mu_T)\nabla\vec{u}\right] + \nabla \cdot \left[-\frac{2}{3}(\bar{\mu} + \mu_T)\nabla\vec{u}\right] + \bar{\rho}\vec{g} \tag{3}$$

$$\frac{\partial(\bar{\rho}h)}{\partial t} + \vec{u} \cdot \nabla(\bar{\rho}h) = \nabla P + \nabla \cdot \left[\left(\frac{\bar{\mu}}{Pr} + \frac{\mu_T}{Pr_T}\right)\nabla h\right] - \nabla q + \dot{\omega}_T + S_h \tag{4}$$

$$\frac{\partial(\bar{\rho}Y_i)}{\partial t} + \vec{u} \cdot \nabla(\bar{\rho}Y_i) = \nabla \cdot \left[\left(\frac{\bar{\mu}}{Sc} + \frac{\mu_T}{Sc_T}\right)\nabla Y_i + D_T\frac{\nabla T}{T}\right] + \dot{\omega}_i \tag{5}$$

Where "P" is pressure, "μ" is dynamic molecular viscosity," μ_t" turbulent dynamic viscosity, "S_h" is heat radiation source "$\dot{\omega}_T$" is the rate of heat release from chemical reactions, " Pr" is the number of molecular Prandtl, "Pr_t" is the number of turbulent Prandtl "$\dot{\omega}_i$"is the rate of production or consumption of species, "Sc" is the number of molecules, and "Sc_t" is the turbulent Schmidt number.

Table 3 Coefficients of k-ε model

σ_ε	σ_k	$C_{3,RDT}$	C_2	C_1
1.3	1.0	0	1.92	1.6

The turbulence model employed was the Reynolds-averaged Navier-Stokes (RANS) approach utilizing the standard k-ε model to account for turbulence effects. Although this model has limitations in accurately predicting round jets, previous research indicated that adjusting the C_1 parameter to 1.60 for self-similar round jets provides good correlation with experimental data [12-15]. This adjustment was applied in all simulations to emphasize the study of turbulence-chemistry interactions while minimizing additional computational complexities.

For the combustion model, the Eddy Dissipation Concept (EDC) was used to analyze the interaction between turbulence and chemical reactions in the furnace. The GRI 3.0 mechanism, which includes 53 species and 325 reactions, was selected to represent the methane oxidation process. To enhance convergence and reduce computational costs, the In-Situ Adaptive Tabulation (ISAT) method was implemented with an error tolerance of 0.00001 to maintain solution accuracy.

The radiation model utilized was the Discrete Ordination (DO) method to solve the Radiative Transfer Equation (RTE), while the Weighted Sum of Gray Gas (WSGG) model was applied to determine the gas absorption coefficient. For numerical schemes, a second-order upwind approach was used for all species variables to improve computational accuracy. Convergence was achieved when two criteria were satisfied: numerical residuals for energy, momentum, and radiation fell below 10^{-6}, and for all other variables, they were below 10^{-6}. Additionally, the maximum and volume-averaged values of temperature, surface-averaged outlet velocity, and volume-averaged oxygen mole fraction showed variations within 1.0 K, 0.1 m/s, and 0.001, respectively.

4 Mesh independency

The analysis of mesh independence and validation of the CFD cases involved solving four meshes with 310,000, 421,000, 595,000, and 842,000 elements. The comparison of these configurations showed that while the mesh with 842,000 elements yielded the most accurate results, it also significantly increased computational costs. In similar conditions, the execution time for the program using 842,000 elements was more than double that of the program with 595,000 elements. However, the results from both configurations were closely aligned, withonly minor differences noted in a few areas, as illustrated in the graphs below (Figures (6)-9). Therefore, a mesh with 595,000 elements was selected for this study. As with all numerical solutions related to combustion, the independence of the temperature distribution, both axially and radially, was first evaluated. Figures (6) and (8) illustrate the strong agreement between the temperature results from the 595,000-element and 842,000-element meshes.

Flow properties, such as velocity, are also critical in flameless combustion, so the mesh independence for velocity was also assessed. This is shown in Figures (7) and (9), where the 595,000-element mesh demonstrates highly accurate velocity results compared to the 40,000-element mesh while providing significant computational efficiency. Thus, the choice of a 595,000-element mesh is well justified in this study.

Figures (6) and (7) confirm that the 595,000-element mesh closely mirrors the performance of the 842,000-element mesh across all regions. Figure (7) displays the generated mesh with 595,000 cells. To achieve an appropriate range of $y+$ on the wall sides, prevent velocity gradients, and satisfy pressure conditions near the inlets and outlets, a finer grid was implemented. This finer mesh was particularly used near the walls of the inlet nozzles and outlet walls through the application of boundary layer meshing.

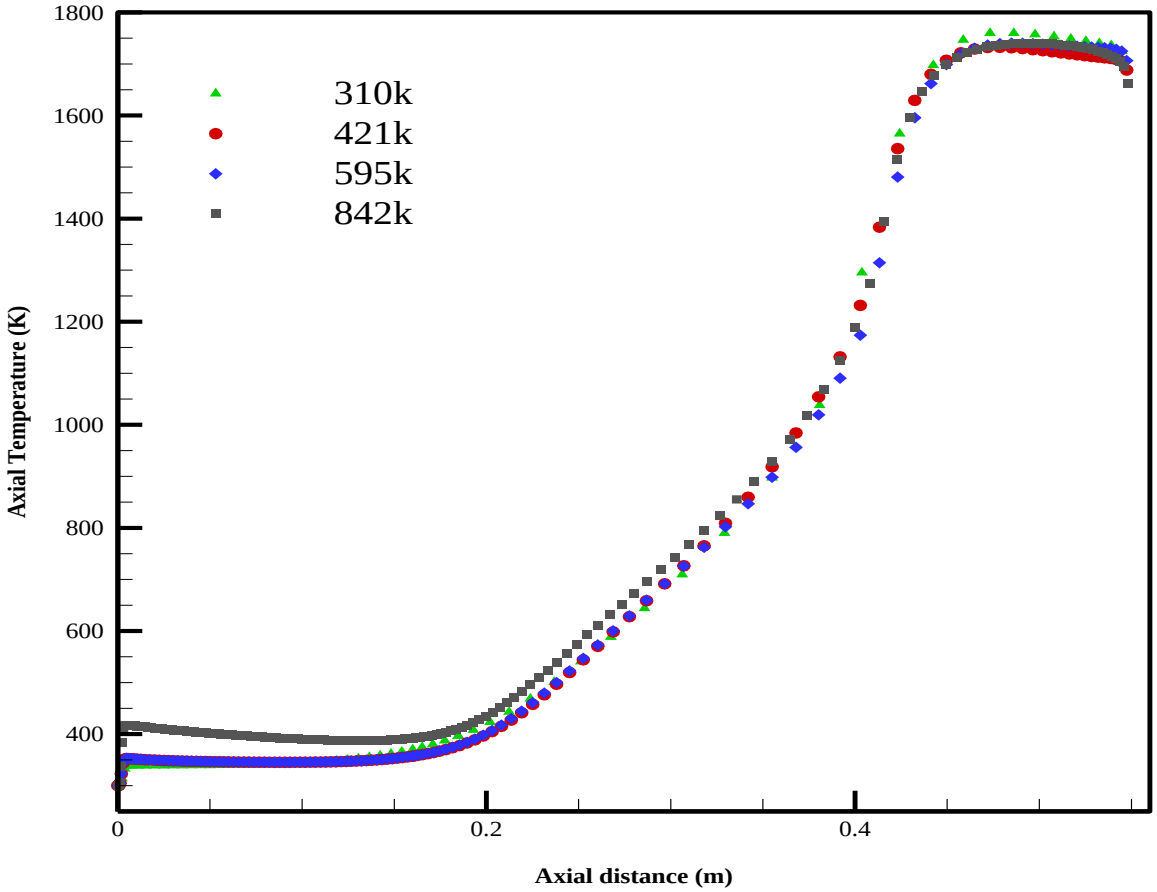

Figure 6 Temperature distribution along the central axis of the furnace for various mesh configurations

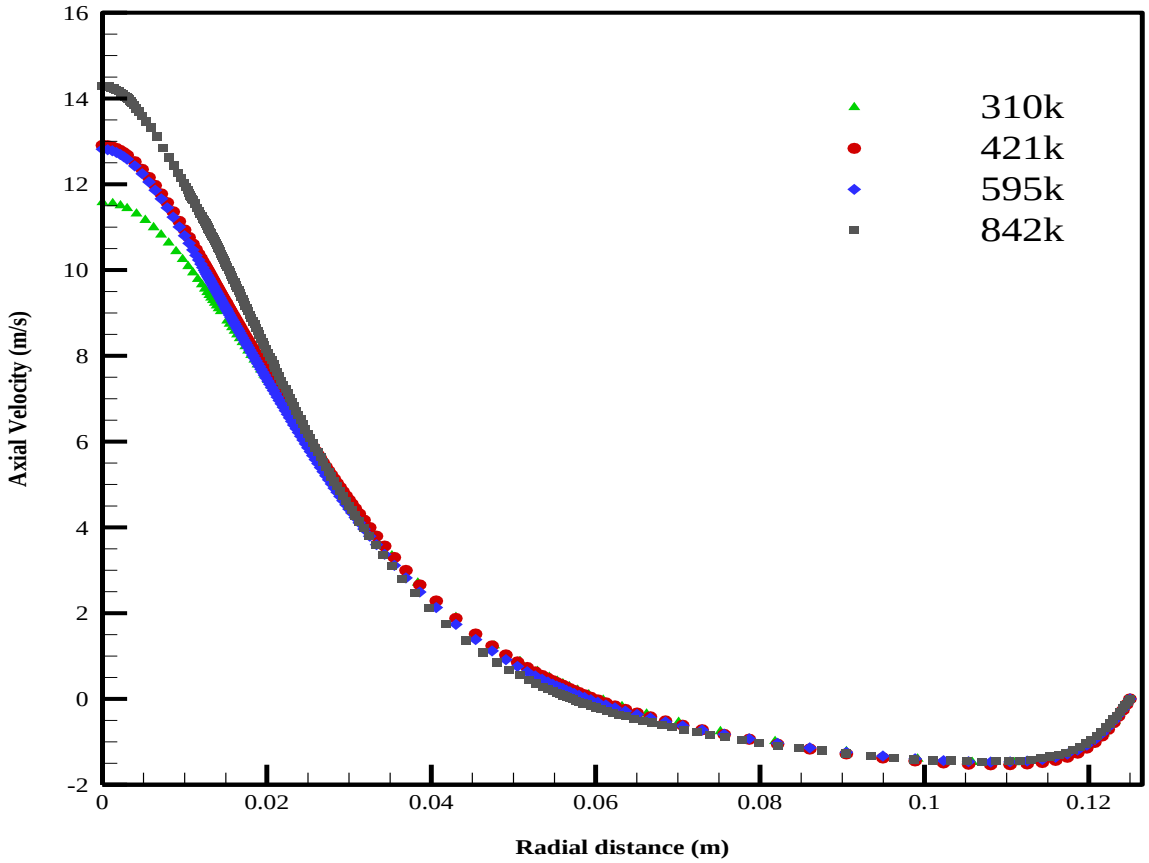

Figure 7 Axial velocity distribution along the central axis of the furnace for different mesh configurations

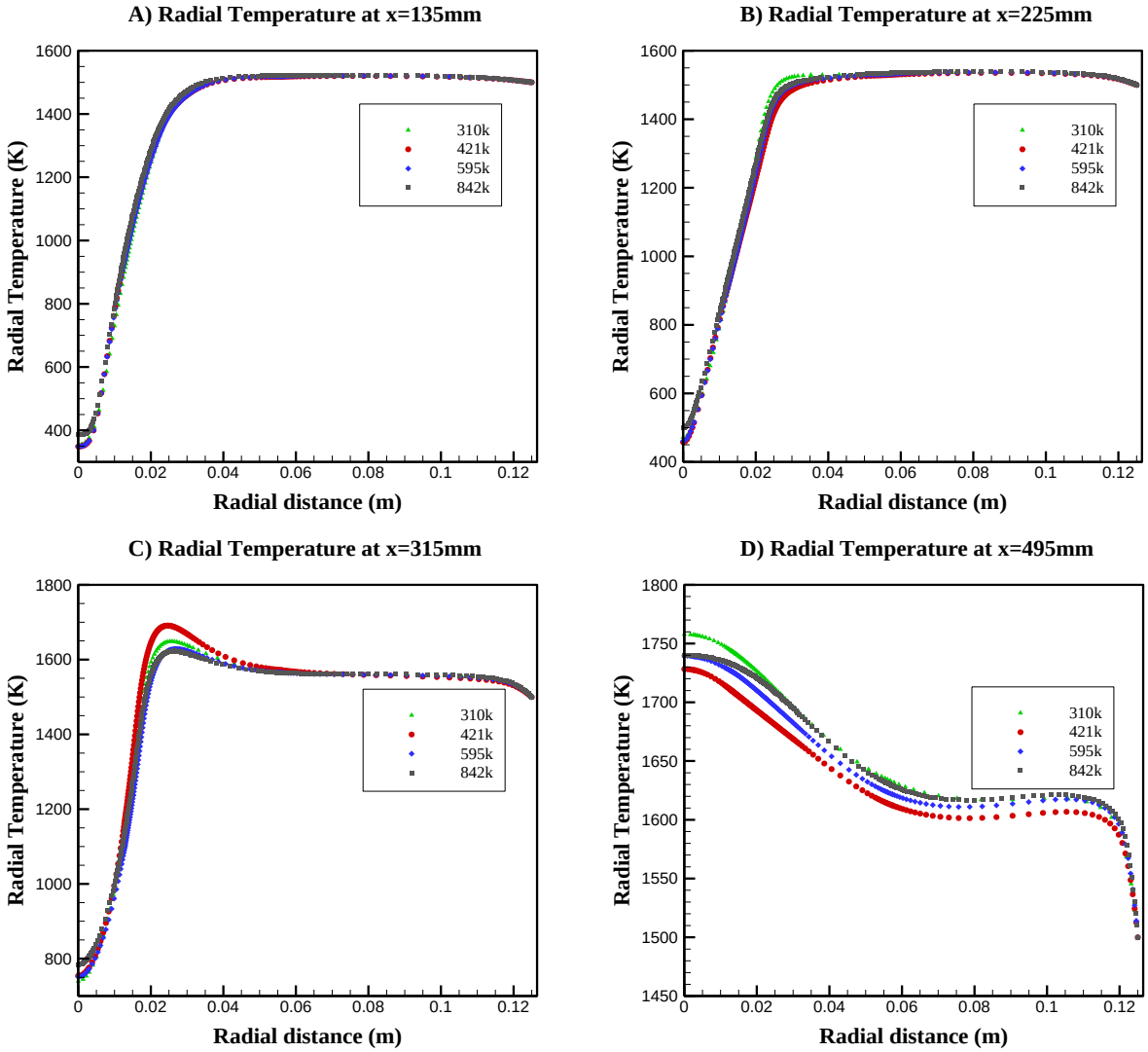

Figure 8 Temperature distribution at different cross-sections of the furnace using multiple mesh configurations

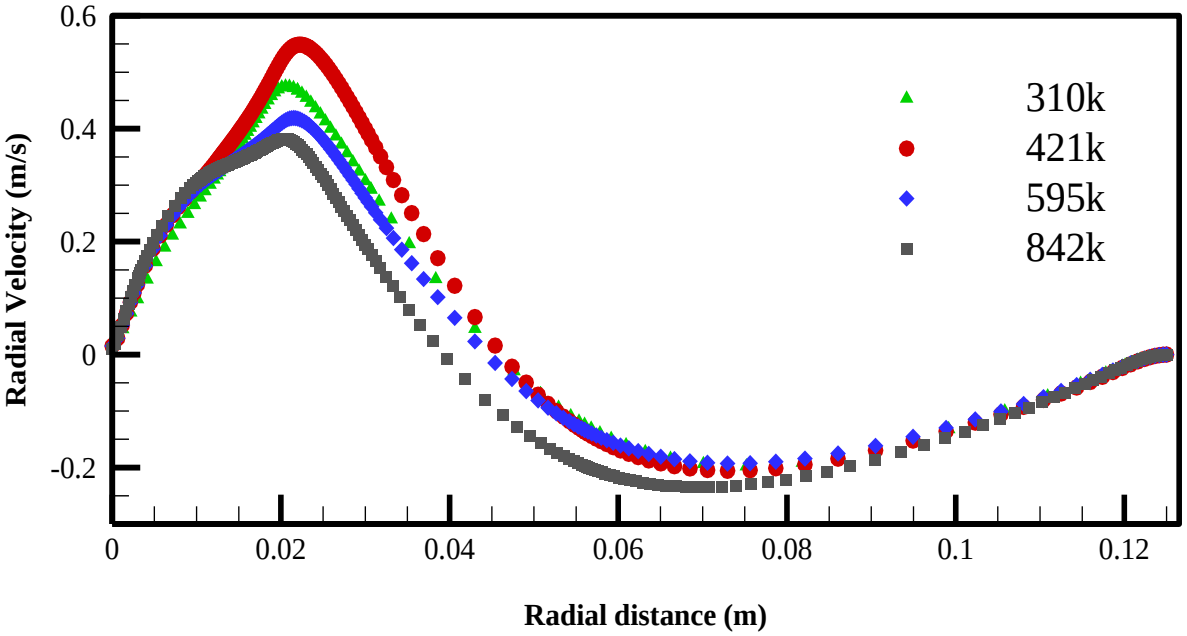

Figure 9 Radial velocity distribution at a cross-section located in the center of the furnace for various mesh configurations

5 Validation

Ansys Fluent 2022-R2 has been used for simulation. To verify the numerical solution, the results of the simulation model are compared with the experimental results of He et.al[16]. Comparison of simulation results with experimental temperature results at different cross-sections and widths is shown in Figure (10). The results show that the difference between simulation results and experimental data is insignificant. The errors between experimental and numerical results in DRM19 and GRI 3.0 are respectively 3.21% and 1.66%, and between the both mechanisms is 1.7%. Therefore, it can be said that the numerical simulation performed in the temperature field has good and consistent accuracy. The DRM19 mechanism predicts more temperatures than the GRI 3.0 mechanism. As shown in Figure (10), the temperature in all sections, especially at higher altitudes, reaches about 1500 K, and by eliminating the temperature gradient, the temperature in the entire chamber is uniform and there aren't any hot spots that disturb the rate of chemical reactions.

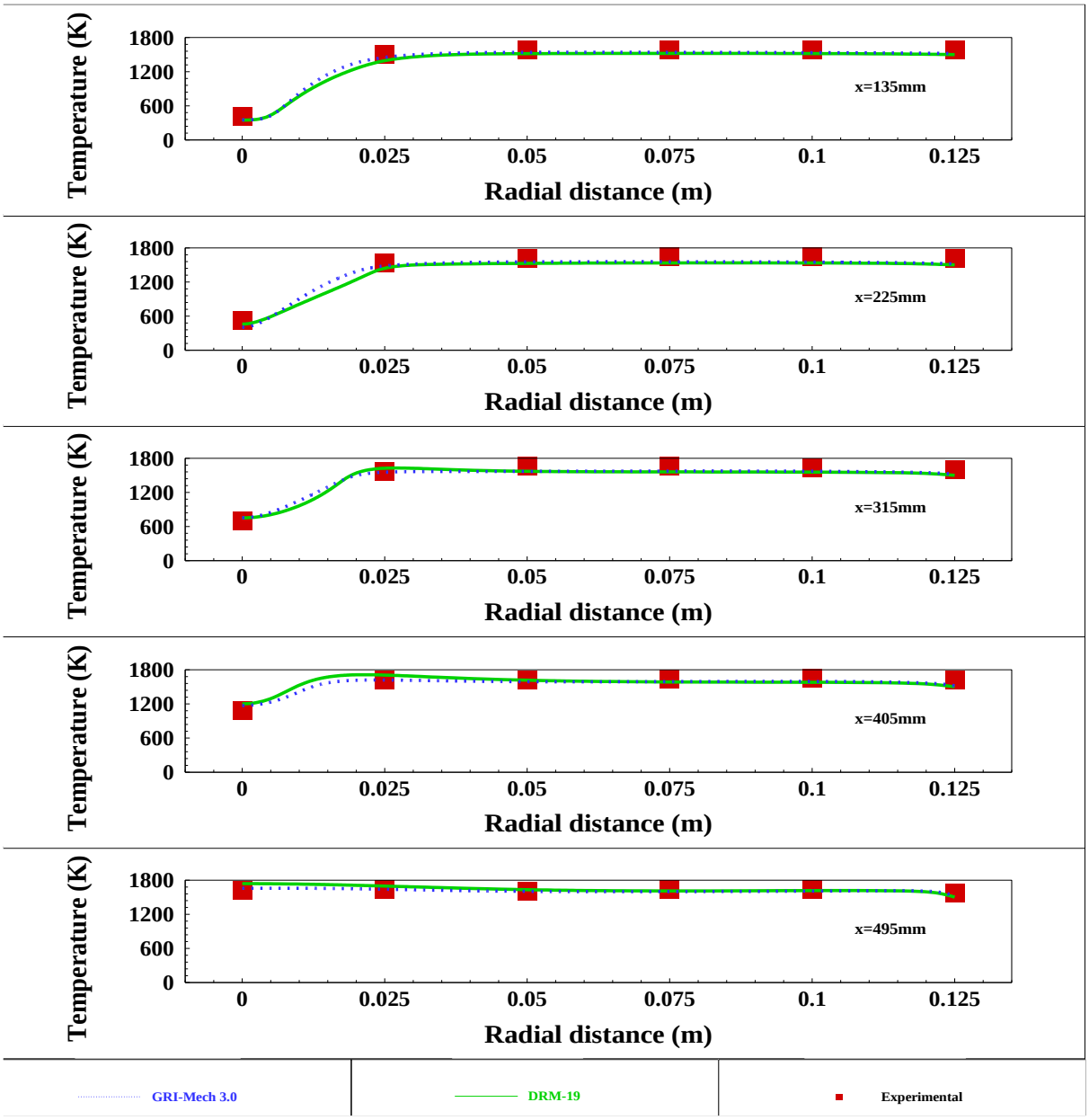

Figure 10 Comparison between the temperature obtained from the numerical simulation and the experimental data [6]

6 Results and discussion

In Figure (11), in the case of carbon monoxide, in some places, especially at low altitudes and near the entrance, there are differences between the numerical and experimental results. For justification, can be said that at low altitudes, carbon monoxide formation dominates the oxidation process, since moving along the chamber, the temperature decreases, oxidation exceeds the formation and Carbon monoxide species are converted into carbon dioxide; therefore, according to Figure (11), the amount of CO decreases along the chamber and reaches approximately less than 5 ppm. The performance of the two combustion mechanisms DRM19 and GRI 3.0 is very close to each other. On average, the error between experimental and numerical results in DRM19 and GRI 3.0 is 36.6% and 45.6%, respectively, the difference between the two mechanisms is 25%, and the DRM19 mechanism predicts the concentration of carbon monoxide is lower than GRI 3.0 mechanism.

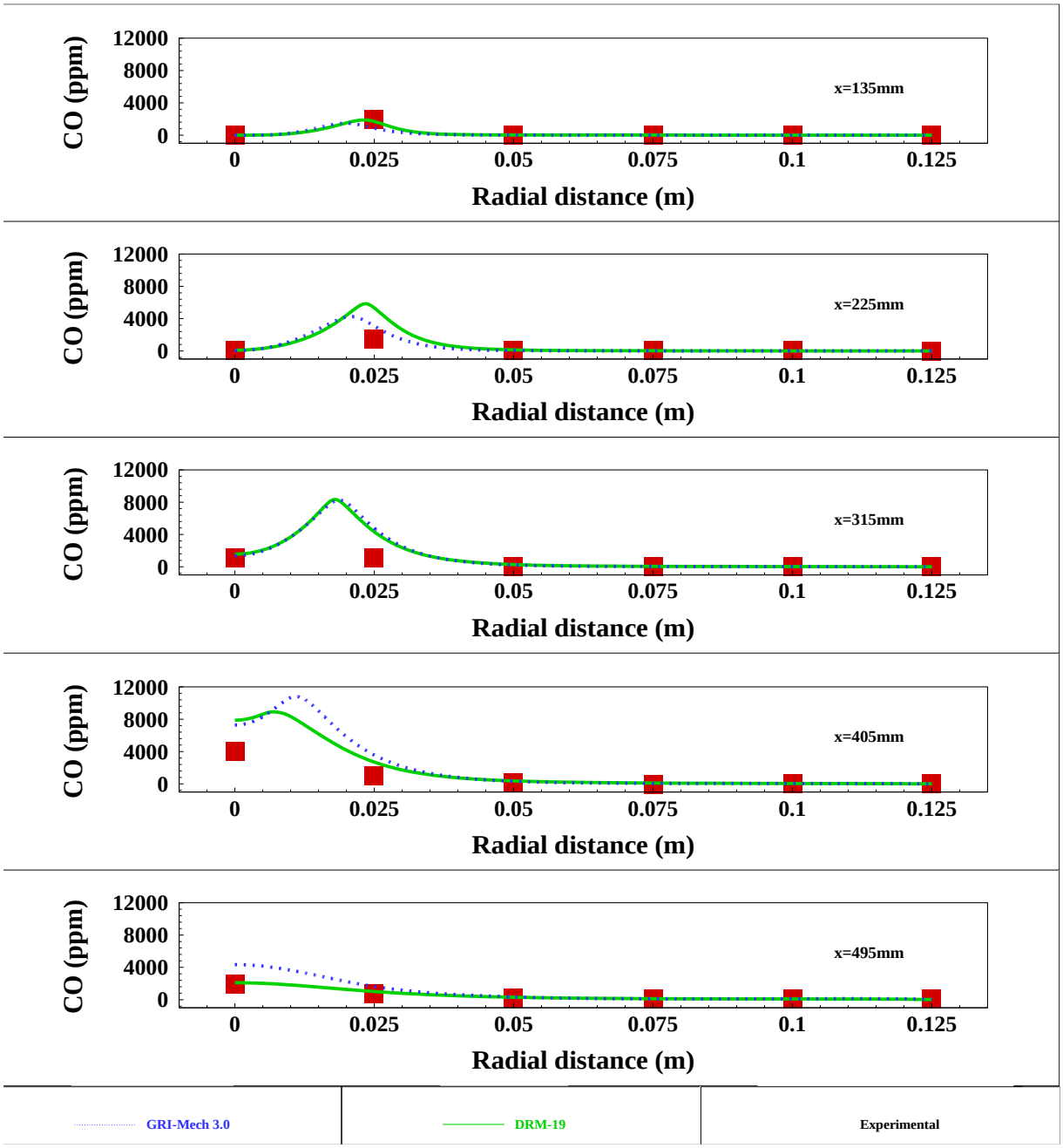

Figure 11 Comparison between the CO values obtained from the numerical simulation and the experimental data [6]

NOx emissions primarily comprise nitric oxide (NO), with smaller proportions of nitrogen dioxide (NO_2) and nitrous oxide (N_2O).
In both laminar flames and the microscopic realm of turbulent flames, the generation of NOx can be ascribed to four distinct chemical kinetic processes: thermal formation, prompt formation, fuel NOx formation, and intermediate N_2O. Thermal NOx arises from the oxidation of atmospheric nitrogen in the combustion air. Prompt NOx is a byproduct of rapid reactions occurring at the flame front. Fuel NOx results from the oxidation of nitrogen present in the fuel. Under heightened pressures and oxygen-rich conditions, NOx may also originate from molecular nitrogen (N_2) through N_2O. The burning and SNCR mechanisms curtail the total NOx formation involving the reaction with hydrocarbons and ammonia, respectively.
As per the conditions outlined in this study, only thermal formation will be elucidated.
ANSYS Fluent addresses the mass transport equation related to the NO species, incorporating factors like convection, diffusion, production, and consumption of NO and its related species. This methodology is highly versatile, stemming from the fundamental principle of mass conservation. The influence of residence time in NOx mechanisms, utilizing a Lagrangian reference frame concept, is integrated through the convection terms within the governing equations framed in the Eulerian reference frame Specifically for thermal mechanisms, the species transport equation stands as the sole requirement [15]:

$$\frac{\partial}{\partial t}(\rho Y_{NO}) + \nabla.\left(\rho \vec{V} Y_{NO}\right) = \nabla.(\rho D \nabla Y_{NO}) + S_{NO} \tag{6}$$

Where Y_{NO} represents the mass fraction of NO in the gas phase, and D is the effective diffusion coefficient. The determination of the source term S_{NO} is carried out in the subsequent steps.
The creation of thermal NOx is governed by a series of chemical reactions highly dependent on temperature, recognized as the extended Zeldovich mechanism. The primary reactions that oversee the generation of thermal NOx molecular nitrogen are as follows[17]:

$$O + N_2 \rightleftharpoons N + NO \tag{7}$$

$$N + O_2 \rightleftharpoons O + NO \tag{8}$$

A third reaction has been demonstrated to play a role in the generation of thermal NOx, especially under near-stoichiometric conditions and in fuel-rich mixtures[17]:

$$N + OH \rightleftharpoons H + NO \tag{9}$$

The rate constants for these reactions have been determined through extensive experimental investigations[18-22] have critically assessed the data derived from these studies. The formulations for the rate coefficients employed in the NOx model, as represented by Eqs (7) - (9) are provided below. These choices were made following the assessment conducted by Hanson and Salimian[22]. In the above expressions, all of these rate constants have units of m^3/(mol-s).

$$\begin{aligned}\frac{d[NO]}{dt} = {} & k_{f.7}[O][N_2] + k_{f.8}[N][O_2] + k_{f.9}[N][OH] \\ & -k_{r.7}[NO][N] - k_{r.8}[NO][O] - k_{r.9}[NO][H]\end{aligned} \tag{10}$$

where the concentrations of all species are expressed in units of mol/m^3.
To compute the rates of NO and N formation, the concentrations of O, H, and OH are necessary.

The NOx formation rate is notable only at elevated temperatures (exceeding 1800 K) because fixing nitrogen involves breaking the robust N_2 triple bond, which has a dissociation energy of 941 KJ/mol. This phenomenon is indicated by the high activation energy in reaction Equation (7), rendering it the rate-determining step in the extended Zeldovich mechanism. Nonetheless, the activation energy for the oxidation of N atoms is low. In the presence of ample oxygen, as seen in a fuel-lean flame, the rate of consumption of free nitrogen atoms equals the rate of their formation, allowing the establishment of a quasi-steady state. This assumption holds true for most combustion scenarios, excluding extremely fuel-rich combustion conditions. Consequently, the NO formation rate becomes:

$$\frac{d[NO]}{dt} = 2k_{f.7}[O][N_2]\frac{\left(1-\frac{k_{r.7}k_{r.8}[NO]^2}{k_{f.7}[N_2]k_{f.8}[O_2]}\right)}{\left(1+\frac{k_{r.7}[NO]}{k_{f.8}[O_2]+k_{f.9}[OH]}\right)} \quad \left(\frac{mol}{m^3-s}\right) \tag{11}$$

As per Equation 1.6, it's evident that the NO formation rate will rise with an increase in oxygen concentration. Additionally, it seems that the thermal formation of NO is significantly influenced by temperature but remains unaffected by the type of fuel. In essence, following the limiting rate defined by $k_{f,7}$, the production rate of thermal NOx doubles for every 90 K increase in temperature beyond 2200 K.

To address Equation 1.6, it will be necessary to have concentrations of atoms and free radicals, along with stable species (that is, O_2, N_2). Following Zeldovich's suggestion, the thermal NOx formation mechanism can be separated from the primary combustion process by assuming equilibrium values for temperature, stable species, O atoms, and OH radicals. However, radical concentrations, especially O atoms, are observed to be higher than their equilibrium levels. The impact of partially equilibrated O atoms on the NOx formation rate has been explored[23]. During laminar methane-air combustion. The findings from these studies suggest that the emission level of NOx can be underestimated by up to 28% in the flame zone when assuming equilibrium O-atom concentrations. To ascertain the concentrations of O radicals and OH radicals, Fluent employs three approaches: Equilibrium, Partial Equilibrium, and Predicted Approach. In this study, the latter is employed. For further details [24-26]. In the Predicted Approach, if the concentration of O atoms (or similarly OH radicals) is accurately predicted using an advanced chemistry model, [O] (or similarly [OH]) can be directly derived from the local O-species mass fraction (or OH mass fraction).

In brief, Equation 1.6 predicts the rate of thermal NOx formation. The O-atom concentration required in Equation 1.6 is calculated using the local O-species mass fraction. Regarding the transport equation for NO Eq. (12), the NO source term attributed to thermal NOx mechanisms is:

$$S_{thermal.NO} = M_{w.NO}\frac{d[NO]}{dt} \tag{12}$$

where $M_{w.NO}$ represents the molecular weight of NO (kg/mol), and d[NO]/dt is derived from Equation (11).

In Figure (12), the NO_X values obtained from simulation and experimental values are given. According to this figure, there is good agreement between the results of the DRM19 mechanism and the experimental results, but GRI 3.0 shows more values than DRM19. The average error between experimental and numerical results in DRM19 and GRI 3.0 is 14.3% and 57.8%, respectively, the difference between the two mechanisms is 26%, and the DRM19 mechanism predicts the nitrogen-oxide concentration is in equilibrium below that level of GRI 3.0. mechanism. However, the maximum NO_X value reached approximately less than 10 ppm, which as expected represents a significant reduction compared to the traditional combustion method.

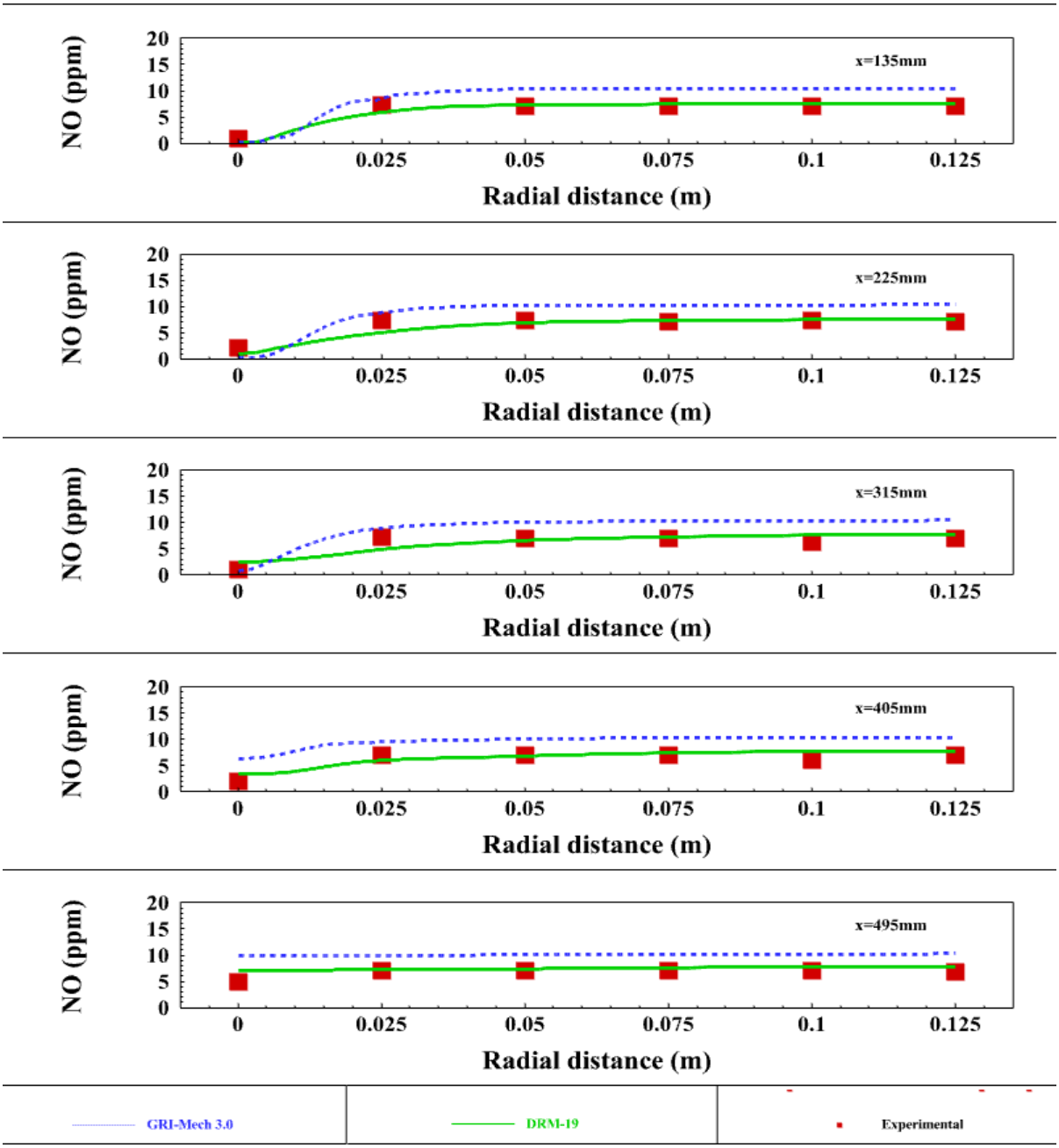

Figure 12 Comparison between the NO_X values obtained from the numerical simulation and the experimental data [6]

7 Conclusions

In this paper, we investigated the efficiency and accuracy of complete and reduced combustion mechanisms in the numerical simulation of MILD combustion. Specifically, we employed two mechanisms: DRM19, which includes 19 species and 84 reactions, and GRI 3.0, comprising 53 species and 325 reactions. Our findings demonstrate that both mechanisms effectively calculate temperature distributions and chemical species concentrations with commendable accuracy when compared to each other and to experimental results.

A notable innovation of this study is the comparative analysis of the reduced DRM19 mechanism against the more complex GRI 3.0 mechanism in MILD combustion scenarios.

This analysis revealed that, while GRI 3.0 predicted NOx concentrations slightly higher than expected, the DRM19 reduction mechanism provided results that are more closely aligned with experimental observations. This suggests that DRM19 not only simplifies the computational process but also retains accuracy, making it a valuable alternative for simulations in MILD combustion applications.

Furthermore, our research highlights the potential of reduced mechanisms in enhancing computational efficiency, especially in large-scale simulations where computational resources may be limited. By demonstrating that DRM19 can achieve results comparable to those of GRI 3.0, we provide a compelling case for the adoption of reduced mechanisms in both academic research and practical engineering applications.

The implications of this work extend beyond mere computational benefits; they also contribute to the understanding of combustion chemistry in MILD conditions. The insights gained from this comparative study can inform future research directions, particularly in optimizing combustion systems to reduce emissions while maintaining performance.

In conclusion, our results indicate that the reduced DRM19 mechanism offers a practical and effective approach for future research and engineering applications, facilitating more efficient simulations without sacrificing accuracy. This study not only advances the field of combustion modeling but also sets the stage for further exploration of reduced mechanisms in various combustion regimes.

References

[1] A. L. N. Stephen, "Center for Strategic and International Studies," Presented at the in *International Energy Outlook 2021 (IEO2021)*, U.S. Energy Information Administration, October 6, Washington, DC 2021, https://scholar.google.com/scholar?hl=fa&as_sdt=0%2C5&q=++International+.

[2] J.A. Wünning, and J.G. Wünning, "Flameless Oxidation to Reduce Thermal Noformation," *Progress in Energy and Combustion Science*, Vol. 23, No. 1, pp. 81-94, 1997, https://doi.org/10.1016/S0360-1285(97)00006-3.

[3] J. Mi, P. Li, F. Wang, K.-P. Cheong, and G. Wang, "Review on MILD Combustion of Gaseous Fuel: Its Definition, Ignition, Evolution, and Emissions," *Energy & Fuels*, Vol. 35, No. 9, pp. 7572-7607, 2021, https://doi.org/10.1021/acs.energyfuels.1c00511.

[4] A. Effuggi, D. Gelosa, and R. Rota, "Mild Combustion in a Laboratory-scale Apparatus," *04 CONTRIBUTO IN ATTI DI CONVEGNO:04. 1 Contributo in Atti di Convegno*, pp, 9-12, 2002, https://hdl.handle.net/11311/567532.

[5] R. Weber, A. K. Gupta, and S. Mochida, "High Temperature Air Combustion (HiTAC): How it All Started for Applications in Industrial Furnaces and Future Prospects," *Applied Energy*, Vol. 278, p. 115551, 2020, https://doi.org/10.1016/j.apenergy.2020.115551.

[6] Y. K. S. Jeon, "Multi-environment Probability Density Function Modeling for Turbulent CH4 Flames under Moderate or Intense Low-oxygen Dilution Combustion Conditions with Recirculated Fue Gases," *Energy & Fuels*, Vol. 31, No. 8, pp. 8685-8697, 2017, https://doi.org/10.1021/acs.energyfuels.7b01060.

[7] K.P. Cheong, G. Wang, J. Si, and J. Mi, "Nonpremixed MILD Combustion in a Laboratory-scale Cylindrical Furnace: Occurrence and Identification," *Energy*, Vol. 216, pp. 119-295, 2021, https://doi.org/10.1016/j.energy.2020.119295.

[8] Z. Li, S. Tomasch, Z. X. Chen, A. Parente, I. S. Ertesvåg, and N. Swaminathan, "Study of MILD Combustion using LES and Advanced Analysis Tools," *Proceedings of the Combustion Institute*, Vol. 38, No. 4, pp. 5423-5432, 2021, https://doi.org/10.1016/j.proci.2020.06.298.

[9] S. Cao, C. Zou, Q. Han, Y. Liu, D. Wu, C. Zheng, "Numerical and Experimental Studies of NO Formation Mechanisms under Methane Moderate or Intense Low-oxygen Dilution (MILD) Combustion without Heated Air," *Energy & Fuels*, Vol. 29, No. 3, pp. 1987-1996, 2015, https://doi.org/10.1021/ef501943v.

[10] T. Poinsot, and D. Veynante, "*Theoretical and Numerical Combustion*," Second Edition, RT Edwards, Inc., Philadelphia, USA, CNRS, ISBN: 1-930217-10-2, [Online], 2011, https://books.google.com/books?hl=fa&lr=&id=cqFDkeVABYoC&oi=fnd&pg=PR11&dq=T.+P.+a.+D.+Veynante,+Theoretical+and+Numerical+Combustion.+CNRS+%5BOnline%5D&ots=LgmWPUHWiD&sig=G4_9DUr7qF13SIdvXkkcHcwuvE#v=onepage&q&f=false.

[11] S. R. Turns, "*An Introduction to Combustion: Concepts and Applications*," 2nd Edition ed., William C Brown Pub: McGraw-Hill Series in Mechanical Engineering, Vol. 287, pp. 569, New York, NY, USA: McGraw-Hill Companies, 2006, https://archive.org/details/introductiontoco0000turn.

[12] G. Khabbazian, J. Aminian, and R. H. Khoshkhoo, "Experimental and Numerical Investigation of MILD Combustion in a Pilot-scale Water Heater," *Energy*, Vol. 239, p. 121888, 2022, https://doi.org/10.1016/j.energy.2021.121888.

[13] S. Xu, S. Xu, Y. Tu, P. Huang, C. Luan, Z. Wang, B. Shi, H. Liu, and Z. Liu, "Effects of Wall Temperature on Methane MILD Combustion and Heat Transfer Behaviors with Non-preheated Air," *Applied Thermal Engineering*, Vol. 174, p. 115282, 2020, https://doi.org/10.1016/j.applthermaleng.2020.115282.

[14] D. He, Y. Yu, Y. Kuang, and C. Wang "Analysis of EDC Constants for Predictions of Methane MILD Combustion," *Fuel*, Vol. 324, p. 124542, 2022, https://doi.org/10.1016/j.fuel.2022.124542.

[15] Fluent A.N., "*Ansys Fluent Theory Guide*", Vol. 15317, pp. 724-746, Nov. 2011, Ansys Inc., USA, [Online] Available: http://scholar.google.com/scholar?hl=en&btnG=Search&q=intitle:ANSYS+FLUENT+Theory+Guide#0.

[16] D. He, Y. Yu, Y. Kuang, and C. Wang, "Analysis of EDC Constants for Predictions of Methane MILD Combustion," *Fuel*, Vol. 324, pp. 124542, 2022, https://doi.org/10.1016/j.fuel.2022.124542.

[17] M. Thiemann, E. Scheibler, and K.W. Wiegand, "Nitric acid, Nitrous acid, and Nitrogen oxides", *Ullmann's Encyclopedia of Industrial Chemistry*, Wiley-VCH Verlag GmbH & Co., 2000, https://doi.org/10.1002/14356007.a17_293.

[18] B. S. J. Blauvens, and J. Peters, "*In 16th Symposium (Int'l.) on Combustion*," The Combustion Institute, Massachusetts Institute of Technology, Cambridge, Mass., August 15-20, Proceedings, Cambridge, MA, 1976, https://scholar.google.com/scholar?hl=fa&as_sdt=0%2C5&q=B.+S.+J.+Blauvens%2C+and+J.+Peters%2C+in+In+16th+Symp.%28Int%E2%80%99l.%29+on+Combustion%2C+1977%3A+The++Combustion+Institute.+&btnG=.

[19] W. L. Flower, R. K. Hanson, and C. H. Kruger, "*In 15th Symp. (Int'l.) on Combustion*," Vol. 823, pp. 160, The Combustion Institute, 1975, https://scholar.google.com/scholar?hl=fa&as_sdt=0%2C5&q=R.+K.+H.+W.+L.+Flower%2C+and+C.+H.+Kruger%2C+in+In+15th+Symp.+%28Int%E2%80%99l.%29+on+Combustion%2C+1979%2C+vol.++823%3A+The+Combustion+Institute.&btnG=.

[20] J. P. Monat, R. K. Hanson, and C. H. Kruger, "*In 17th Symp. (Int'l.) on Combustion*," 1979, pp. 543, The Combustion Institute, https://scholar.google.com/scholar?hl=fa&as_sdt=0%2C5&q=R.+K.+H.+J.+P.+Monat%2C+and+C.+H.+Kruger%2C+in+In+17th+Symp.+%28Int%E2%80%99l.%29+on+Combustion%2C+1979%2C+vol.++543%3A+The+Combustion+Institute.&btnG=.

[21] D. L. Baulch, M. Bowers, D. G. Malcolm, and R. T. Tuckerman, "Evaluated Kinetic Data for High-temperature Reactions", Vol. 5, Part 1, Homogeneous Gas Phase Reactions of the Hydroxyl Radical with Alkanes," *Journal of Physical and Chemical Reference Data*, Vol. 15, No. 2, pp. 465-592, 1986, https://doi.org/10.1063/1.555774.

[22] R. K. Hanson, and S. Salimian, "*Survey of Rate Constants in the N/H/O System*," In Combustion Chemistry: Springer, New York: Springer New York, NY, pp. 361-421, 2018, https://link.springer.com/chapter/10.1007/978-1-4684-0186-8_6.

[23] T. J. Foster, C. W. Wilson, M. Pourkashanian, and A. Williams, "3D Modelling of NOx Emissions from an Aircraft Afterburner", *American Society of Mechanical Engineers (ASME), International Gas Turbine and Aeroengine Congress and Exhibition*, Vol. 78590, pp. V002T02A060, June 7–10, Indianapolis, Indiana, USA, 1999.

[24] M. C. Drake, S. M. Correa, R. W. Pitz, W. Shyy, and C. P. Fenimore, "Superequilibrium and Thermal Nitric oxide Formation in Turbulent Diffusion Flames," *Combustion and Flame*, Vol. 69, No. 3, pp. 347–365, 1987, https://doi.org/10.1016/0010-2180(87)90126-X.

[25] A. Westenberg, "Kinetics of NO and CO in Lean, Premixed Hydrocarbon-air Flames," *Combustion Science and Technology*, Vol. 4, No. 1, pp. 59-64, 1971, https://doi.org/10.1080/00102207108952472.

[26] J. Warnatz, "*NOx Formation in High Temperature Processes*," University of Stuttgart, Stuttgart, Germany, 2001, https://scholar.google.com/scholar?hl=fa&as_sdt=0%2C5&q=J.+Warnatz%2C+%22NOx+Formation+in+HighTemperature+Processes.%22+Germany%3A+University+of++Stuttgart&btnG=.

Nomenclature

English symbols

D	Diffusivity, (m^2/s)
g	Gravity acceleration, (m/s^2)
h	Specific enthalpy, (KJ/kg)
P	Pressure, (Pa)
q	Heat flux, (W/m^2)
t	Time, (s)
u, V	Velocity, (m/s)
Y	Mole fraction, (-)

Greek symbols

λ	Excess air, (-)
μ	Dynamic viscosity, (Pa.s)
ρ	Density, (Kg/m^3)
ω	Chemical reaction rate, (Kmol/s)